

Document downloaded from:

<http://hdl.handle.net/10251/171683>

This paper must be cited as:

Cerqueira, A.; Romero-Gavilán, F.; Araujo-Gomes, N.; García-Arnáez, I.; Martínez-Ramos, C.; Ozturan, S.; Azkargorta, M.... (2020). A possible use of melatonin in the dental field: Protein adsorption and in vitro cell response on coated titanium. *Materials Science and Engineering C: Materials for Biological Applications* (Online). 116:1-10.
<https://doi.org/10.1016/j.msec.2020.111262>



The final publication is available at

<https://doi.org/10.1016/j.msec.2020.111262>

Copyright Elsevier BV

Additional Information

1 **A possible use of melatonin in the dental field: protein adsorption and *in vitro* cell response**
2 **on coated titanium**

3 Andreia Cerqueira¹, Francisco Romero-Gavilán^{1*}, Nuno Araújo-Gomes², Iñaki García-Arnáez³,
4 Cristina Martínez-Ramos⁴, Seda Ozturan⁵, Mikel Azkargorta⁶, Félix Elortza⁶, Mariló
5 Gurruchaga³, Julio Suay¹, Isabel Goñi³

6 ¹Department of Industrial Systems Engineering and Design, Universitat Jaume I, Av. Vicent Sos
7 Baynat s/n, 12071 Castellón de la Plana, Spain

8 ²Department of Developmental Bioengineering, University of Twente, Faculty of Science and
9 Technology, 7522LW, Enschede, The Netherlands

10 ³Facultad de Ciencias Químicas, Universidad del País Vasco, P. M. de Lardizábal, 3, 20018 San
11 Sebastián, Spain

12 ⁴Center for Biomaterials and Tissue Engineering, Universitat Politècnica de Valencia, Camino de
13 Vera, s/n 46022 Valencia, Spain

14 ⁵Department of Periodontology, Faculty of Dentistry, Istanbul Medeniyet University, Istanbul,
15 Turkey

16 ⁶Proteomics Platform, CIC bioGUNE, CIBERehd, ProteoRed-ISCI, Bizkaia Science and
17 Technology Park, 48160 Derio, Spain

18 *Corresponding author: Francisco Romero-Gavilán

19 Departamento de Ingeniería de Sistemas Industriales y Diseño

20 Campus del Riu Sec

21 Avda. Vicent Sos Baynat s/n

22 12071 – Castelló de la Plana (España)

23 E-mail: gavilan@uji.es

24

25

26

27

28

29

30 **Abstract**

31 Melatonin (MLT) is widely known for regulating the circadian cycles and has been studied for its
32 role on bone regeneration and inflammation. Its application as coating for dental implants can
33 condition the local microenvironment, affecting protein deposition on its surface and the cellular
34 and tissue response. Using sol-gel coatings as a release vehicle for MLT, the aim of this work was
35 assessing the potential of this molecule in improving the osseointegration and inflammatory
36 responses of a titanium substrate. The materials obtained were physicochemically characterized
37 (scanning electron microscopy, contact angle, roughness, Fourier-transform infrared
38 spectroscopy, nuclear magnetic resonance, Si release, MLT liberation and degradation) and
39 studied *in vitro* with MC3T3-E1 osteoblastic cells and RAW264.7 macrophage cells. Although
40 MLT application did not improve osteoblastic cells behavior, it presented an anti-inflammatory
41 potential, and effects in coagulation and angiogenesis pathways depending on the dosage used.
42 Using LC-MS/MS, protein adsorption patterns were studied after incubation with human serum.
43 Proteins related with the complement systems (CO7, IC1, CO5, CO8A, and CO9) were less
44 adsorbed in materials with MLT; on the other hand, proteins with functions in the coagulation
45 and angiogenesis pathways, such as A2GL and PLMN, showed a significant adsorption pattern.

46 **Keywords**

47 Osseointegration, hybrid sol-gel, inflammation, proteomics, coating, *N*-acetyl-5-metoxi-
48 tryptamine

49 **1. Introduction**

50 Dental implantations have become a standard procedure in oral rehabilitation, representing a
51 reliable treatment with many advantages. However, implant failure still occurs, particularly in
52 patients with poor osseointegration capability (*e.g.* patients with osteoporosis), prompting the
53 need for bioactive surfaces that accelerate this process[1].

54 Titanium (Ti) and its alloys are commonly used in dental implants due to their high degree of
55 biocompatibility. However, these materials have the limitation of being relatively bioinert and
56 various methodologies are being studied to confer them bioactive properties. The sol-gel
57 technique allows the synthesis of coatings to metal surfaces with a variety of functions, being an
58 attractive method due to the use of mild reaction conditions, easily available precursors and their
59 potential as controlled release vehicles for ions and biomolecules[2]. Using modified
60 alkoxysilanes as precursors, Martínez-Ibañez et al.³ obtained a sol-gel material by the mixture of
61 methyltrimetoxisilane (MTMOS) and tetraethyl orthosilicate (TEOS) precursors, in a proportion
62 of 70% MTMOS to 30% TEOS, presenting promising cellular *in vitro* behavior, with the

63 improvement of the osseointegrative properties regarding the non-coated sand-blasted acid-
64 etched titanium.

65 Melatonin (*N*-acetyl-5-methoxy-tryptamine; MLT), a widely known regulator of the circadian
66 cycles produced by the pineal gland, has been described to play a major role on bone physiology
67 through dual actions on osteoblasts and osteoclasts[4]. Previous studies[5–8] show that MLT
68 upregulates the gene expression of RUNX2, BMP2, BMP6 and OCN, which have a pivotal role
69 in osteoblast function and bone mineralization. On the other hand, MLT downregulates the
70 expression of RANKL and upregulates OPG, leading to a restriction of osteoclast formation and
71 increment of bone regeneration[9]. Additionally, MLT has been studied for its anti-inflammatory
72 potential leading to the downregulation of TNF α , IL-1 β , IL-6[10,11], and iNOS[11,12].
73 Considering the effects of this molecule in bone and inflammatory responses, MLT has become
74 a particularly attractive molecule to use in implants.

75 Upon implantation, blood/implant interactions lead to immediate protein adsorption onto the
76 implant surface, and consequently developing a provisional matrix on and around the biomaterial.
77 The type, level, and surface conformation of the adsorbed proteins will determine the biological
78 response and the ultimate implant outcome[13]. This adsorption is dependent on surface
79 properties of the material, such as wettability, roughness, and charge [14,15]. Thus, these
80 parameters can ultimately have a determining role not only in the initial immune responses but
81 also in other processes, such as coagulation, fibrinolysis, and the earlier stages of
82 osteogenesis[16].

83 In this work, a new sol-gel material doped with several percentages of MLT (1%, 5%, 7.5% and
84 10%) to be applied as coating onto titanium substrates were developed. Then, we proceeded to
85 perform its physiochemical study, *in vitro* characterization with MC3T3-E1 osteoblasts and RAW
86 264.7 macrophages, and protein adsorption patterns evaluation using proteomics. The main goal
87 was to evaluate the potential of MLT when applied on titanium substrates for future dental field
88 use.

89 **2. Materials and methods**

90 **2.1. Sol-gel synthesis and sample preparation**

91 The sol-gel route was used to obtain hybrid coatings with different percentages of MLT (1%, 5%,
92 7.5% and 10%) using MTMOS and TEOS (Sigma-Aldrich, St. Louis, MO, USA) as precursors.
93 The network contained 70 and 30% (molar percentages) of these precursors, respectively.
94 Melatonin was dissolved in 2-Propanol (Sigma-Aldrich, St. Louis, MO, USA) and mixed with
95 the precursors in a volume ratio (alcohol:siloxane) of 1:1. The hydrolysis of alkoxysilanes was
96 carried out by adding (at a rate of 1-drop s⁻¹) the corresponding stoichiometric amount of aqueous
97 solution of 0.1N HCl (Sigma-Aldrich, St. Louis, MO, USA). The preparations were kept under

98 stirring for 1 h and then 1 h at rest. Afterwards, grade-4 Ti discs (12-mm diameter, 1-mm thick)
99 with a sandblasted acid etched treatment as described by Romero-Gavilán et al. [16] were used
100 as coating substrate. SAE-titanium discs were coated with a dip-coater (KSV DC; KSV NIMA,
101 Espoo, Finland). The discs were immersed in the sol-gel solutions at a speed of 60 cm min⁻¹, left
102 immersed for one minute, and removed at a 100 cm min⁻¹. In order to measure hydrolytic
103 degradation and silicon/MLT liberations, coatings were prepared using glass-slides as a substrate.
104 These were previously cleaned in an ultrasonic bath (Sonoplus HD 3200) for 20 min at 30 W with
105 nitric acid solution (25% volume), and then, with distilled water under the same conditions. In
106 addition, free films of distinct materials were obtained by pouring the sol-gel solutions into non-
107 stick Teflon molds in order to carry out their chemical characterization. Finally, all samples were
108 cured for 2 h at 80°C.

109 **2.2. Physicochemical characterization**

110 To evaluate how surface topography was modified by MLT incorporation, scanning electron
111 microscopy (SEM) with a Leica–Zeiss LEO equipment under vacuum (Leica, Wetzlar, Germany)
112 was used. Before observation, the materials were treated with platinum sputtering to increase their
113 conductivity. To measure surface roughness, an optical profilometer (interferometric and
114 confocal) PLm2300 (Sensofar, Barcelona, Spain) was used in three discs of each material. For
115 each disc, three measurements were done to calculate the average values of the Ra parameter. The
116 contact angle was measured using an automatic contact angle meter OCA 20 (DataPhysics
117 Instruments, Filderstadt, Germany). An aliquot of 10 µL of Milli-Q water was deposited on the
118 disc surface at a dosing rate of 27.5 µL s⁻¹ at room temperature. Contact angles were determined
119 using the SCA 20 software (DataPhysics Instruments, Filderstadt, Germany). Six discs of each
120 material were studied after depositing two drops on each disc.

121 To chemically characterize all materials, Fourier Transform Infrared Spectroscopy (FTIR;
122 Thermo Nicolet 6700) was carried out with an attenuated total reflection system (ATR). The
123 spectra were measured in the 4000 and 400 cm⁻¹ wavelength range. Solid-state silicon nuclear
124 magnetic resonance spectroscopy (²⁹Si-NMR; Bruker 400 Avance III WB Plus) with a probe for
125 solid samples of ICP-MS was used to evaluate the crosslinking degree of the obtained silicon
126 networks. The pulse sequence for the analysis was the Bruker standard: 79.5 MHz frequency,
127 spectral width of 55 KHz, 2 ms contact time and 5 s delay time. The spinning speed was 7.0 kHz.
128 Hydrolytic degradation was evaluated by sample measuring weight loss before and after soaking
129 them in 50 mL of distilled water (ddH₂O) at 37°C during 1, 2, 4 and 8 weeks. The degradation
130 of the coatings was registered by percentage (%) of mass lost in reference to the initial weight.
131 Each data point is the average of three measurements performed in three different samples
132 identically prepared.

133 To determine Si release, samples were incubated in 50 mL of Milli-Q water at 37°C during 1, 2,
134 4 and 8 weeks. At these measuring points, aliquots of 50 µL were taken and measured using
135 inductively coupled plasma mass spectrometry (ICP-MS, Agilent 7700). To measure MLT
136 release, coated glass slides were submerged in 50 mL of Milli-Q water at 37°C. At 0, 1, 3, 5, 8,
137 24, 48, 72, 96, 168 and 336 hours the absorbance was measured at 222 nm (wavelength
138 characteristic of MLT [17]) with a Helios Omega UV-VIS (Thomas Scientific, New Jersey,
139 USA). The measurements were carried out in triplicate.

140 **2.3. *In vitro* assays**

141 **2.3.1. Cell culture**

142 Mouse calvaria osteosarcoma MC3T3-E1 cells and mouse murine macrophage RAW 264.7 cells
143 were cultured in at 37°C in a humidified (95%) CO₂ incubator in Dulbecco's Modified Eagle
144 Medium (DMEM; Gibco, Life Technologies, Thermo Fisher Scientific, NY, USA) supplemented
145 with 1% penicillin/streptomycin (Biowest Inc., USA) and 10% FBS (Gibco, Life Technologies,
146 Grand Island, NY, USA). After 24h, the MC3T3-E1 cells medium was replaced by osteogenic
147 medium composed of DMEM, 1% of penicillin/streptomycin, 10% FBS, 1% ascorbic acid (5
148 mg/mL) and 0.21% β-glycerol phosphate. The culture medium was changed every other day. In
149 each plate, wells with only cells were used as a control of culture conditions.

150 **2.3.2. Cytotoxicity**

151 Biomaterial cytotoxicity was assessed following the ISO 10993-5:2009 (Annex C) norm.
152 MC3T3-E1 cells (1x10⁴ cells/well) were seeded on 96-well NUNC plates (Thermo Fisher
153 Scientific, Waltham, MA, USA) for 24h. The materials were also incubated for 24h in 48-well
154 NUNC plates (Thermo Fisher Scientific) in DMEM with 1% of penicillin/streptomycin and 10%
155 FBS. Then, the cell culture medium was replaced with the medium exposed to the materials
156 followed by an incubation of 24h. To measure cell viability, the CellTiter 96® Proliferation Assay
157 (MTS) (Promega, Madison, WI) was used according to manufacturer's guidelines. As a negative
158 control, wells with only cells were used. As a positive control, cells were incubated in latex, a
159 compound well known for being cytotoxic. A material was considered cytotoxic when presented
160 a cell viability below 70%.

161 **2.3.3. Cell proliferation**

162 To measure the effects of the biomaterials in cell proliferation, the alamarBlue™ cell viability
163 reagent (Invitrogen, Thermo Fisher Scientific, Waltham, MA, USA) was used. MC3T3-E1 cells
164 were cultured in 24-well NUNC plates (Thermo Fisher Scientific, Waltham, MA, USA) at a
165 density of 3.5x10⁴ cells cm⁻². After culturing for 1, 3 and 7 days, cell proliferation was evaluated
166 following the manufacturer's protocol.

167 **2.3.4. Alkaline phosphatase activity assay**

168 To evaluate the effects of the materials in the mineralization capability of osteoblastic cells, the
169 conversion of *p*-nitrophenylphosphate (*p*-NPP) to *p*-nitrophenol was used to assess the alkaline
170 phosphatase (ALP) activity. MC3T3 cells were seeded onto the distinct surfaces in 24-well
171 NUNC plates (Thermo Fisher Scientific, Waltham, MA, USA) at a density of 3.5×10^4 cells cm^{-2} .
172 After culturing for 14 and 21 days, cells were rinsed twice with Dulbecco's phosphate-buffered
173 saline (DPBS; Thermo Fisher Scientific, NY, USA), immersed in lysis buffer (0.2% Triton X-
174 100, 10 mM Tris-HCl, pH 7.2) and incubated at 4°C for 10 minutes. Following centrifugation (7
175 min, 14000 rpm, 4°C), 100 μL of *p*-NPP (1mg mL^{-1}) in substrate buffer (50 mM glycine, 1 mM
176 MgCl_2 , pH 10.5) was added to 100 μL of the supernatant. After 2h of incubation in the dark (37°C,
177 5% CO_2), the absorbance at 405 nm was measured using a microplate reader. Alkaline
178 phosphatase activity was calculated using a *p*-nitrophenol in 0.02 mM sodium hydroxide standard
179 curve. A Pierce BCA assay kit (Thermo Fisher Scientific, Waltham, MA, USA) was used to
180 calculate total protein content in the sample and to normalize ALP levels. The experiment was
181 carried out in triplicate.

182 **2.3.5. RNA extraction and cDNA synthesis**

183 To evaluate the effects on the gene expression of osteogenic and inflammatory targets, MC3T3-
184 E1 cells were seeded on the discs in 48-well NUNC plates (Thermo Fisher Scientific) at a density
185 of 3.5×10^4 cells cm^{-2} for 7 and 14 days, while RAW264.7 were seeded at a density of 30×10^4 cells
186 cm^{-2} for 1 day and 1.5×10^4 cells cm^{-2} for 3 days. In each plate, wells without any material were
187 used as control of culture conditions. Total RNA was extracted using TRIzol (1M guanidine
188 thiocyanate, 1M ammonium thiocyanate, 3M sodium acetate, 5% glycerol, 38% aquaphenol).
189 Briefly, 300 μL of TRIzol were added to which well and incubated at room temperature for 5
190 minutes. Following centrifugation (5 min, 13000 rpm, 4°C), the supernatant was transferred, 200
191 μL of chloroform were added, and the samples were centrifuged (5 min, 13000 rpm, 4°C). The
192 aqueous layer was mixed with 550 μL of isopropanol and kept at room temperature for 10 min.
193 Samples were centrifuged (15 min, 13000 rpm, 4°C) and washed twice with 0.5 mL of 70%
194 ethanol. The resulting pellet was dissolved in 30 μL of RNase free-water. RNA concentration,
195 integrity, and quality were measured using NanoVue® Plus Spectrophotometer (GE Healthcare
196 Life Sciences, Little Chalfont, United Kingdom). For cDNA synthesis, approximately 1 μg of
197 total RNA was converted into cDNA using PrimeScript RT Reagent Kit (Perfect Real Time)
198 (TAKARA Bio Inc., Shiga, Japan) in a reaction volume of 20 μL . The reaction was conducted in
199 (xxx) with the following conditions: 37°C for 15 min, 85°C for 5 secs and a final hold at 4°C. The
200 resulting cDNA quality and concentration was measured using a NanoVue® Plus
201 Spectrophotometer (GE Healthcare Life Sciences), then diluted in DNase-free water to a

202 concentration suitable for reliable qRT-PCR analysis and stored at -20°C until further analysis.
 203 The experiment was carried out in quadruplicate.

204 **2.3.6. Quantitative real-time PCR**

205 Quantitative real-time PCRs (qRT-PCR) were carried out on 96-well plates (Applied
 206 Biosystems®, Thermo Fisher Scientific, Waltham, MA, USA) with each sample represented by
 207 the gene of interest and one housekeeping gene (*glyceraldehydephosphate dehydrogenase*
 208 (GAPDH)). Primers for each gene were designed using PRIMER3plus software tool
 209 (<http://www.bioinformatics.nl/cgi-bin/primer3plus/primer3plus.cgi>) from specific DNA
 210 sequences obtained from NCBI (<https://www.ncbi.nlm.nih.gov/nucleotide/>) and purchased to
 211 Thermo Fischer Scientific. Targets studied were are shown in **Table 1-**. Individual reactions
 212 contained 1 µL of cDNA, 0.2 µL of specific primers (forward and reverse at a concentration of
 213 10 µM L⁻¹) and 5 µL of SYBR Premix Ex Taq (Tli RNase H Plus) (TAKARA) in a final volume
 214 of 10 µL. Reactions were carried out in a StepOne Plus™ Real-Time PCR System (Applied
 215 Biosystems®, Thermo Fisher Scientific, Waltham, MA, USA) . at 95°C for 30s, followed by 40
 216 cycles of 95°C for 5s, 60°C for 34s, 95°C for 15s and 60°C for 60s. The data were obtained using
 217 the StepOne Plus™ Software 2.3 (Applied Biosystems®, Thermo Fisher Scientific, Waltham,
 218 MA, USA). Fold changes were calculated using the 2^{-ΔΔCt} method and the data was normalized
 219 in relation to the blank wells (without any material). Six technical replicates for each sample were
 220 measured.

221 **Table 1:** Quantitative real-time PCR primer sequence.

Gene symbol	Sequence	Accession number	Product length
Both cell lines			
<i>GAPDH</i>	F: TGCCCCCATGTTTGTGATG R: TGGTGGTGCAGGATGCATT	XM_017321385	83
MC3T3-E1			
<i>BGLAP</i>	F: AAGCAGGAGGGCAATAAGGT R: TGCCAGAGTTTGGCTTTAGG	NM_001032298	212
RAW264.7			
<i>IL1BETA</i>			

222

223 **2.3.7. Cytokine quantification by ELISA**

224 To evaluated the influence of the materials in tumor necrosis factor (TNF)- α and interleukin 4
225 (IL-4) production, RAW264.7 cells were seeded in 48-well NUNC plates (Thermo Fisher
226 Scientific, Waltham, MA, USA) a density of 30×10^4 cells cm^{-2} for 1 day and and 1.5×10^4 cells
227 cm^{-2} for 3 days. Then, the cell culture media was collected and frozen until further analysis. The
228 concentration of these cytokines was determined using an ELISA (Invitrogen, Thermo Fisher
229 Scientific, Waltham, MA, USA) kit and according to the manufacturer's instructions.

230 **2.3.8. Adsorbed protein layer**

231 For obtaining the proteins adsorbed by the material surface, discs doped with MLT were incubated
232 for 3 h (37 °C, 5% CO₂) in 24-well NUNC plates (Thermo Fisher Scientific, Waltham, MA, USA)
233 with 1 mL of human blood serum from male AB plasma (Sigma–Aldrich, Merck KGaA,
234 Darmstadt, Germany). After incubation, the serum was removed and the discs were washed five
235 times with ddH₂O and once with 100 mM NaCl, 50 mM Tris–HCl, pH 7.0 to eliminate non-
236 adsorbed proteins. The materials were washed once with an elution (0.5 M triethylammonium
237 bicarbonate buffer (TEAB), 4% of sodium dodecyl sulfate (SDS), 100 mM of dithiothreitol
238 (DTT)) to obtain the adsorbed protein layer. Four independent replicates were analyzed for each
239 surface and each replicated was a pull of four discs. **The analysis was made in four independent**
240 **replicates and each replicate was a pool of four discs.** A Pierce BCA assay kit (Thermo Fisher
241 Scientific,) was used to calculate total protein content in the serum.

242 **2.3.9. Proteomic analysis**

243 Proteomic analysis was performed as described by Romero-Gavilán et al. [16] with slight
244 modifications. Briefly, the eluted protein was digested in-solution, following the FASP protocol
245 established by Wiśniewski et al. [18], and loaded onto a nanoACQUITY UPLC system (Waters,
246 Milford, MA, USA) connected online to a mass spectrometer (Thermo Fisher, Bremen,
247 Germany). Each material was analyzed in quadruplicate. Differential protein analysis was carried
248 out using Progenesis software (Nonlinear Dynamics, Newcastle, UK) as described before
249 Romero-Gavilán et al. [16], and the functional annotation of the proteins was performed using
250 DAVID Go annotation program (<https://david.ncifcrf.gov/>) and PANTHER classification system
251 (<http://www.pantherdb.org/>).

252

253

254 **2.4. Statistical analysis**

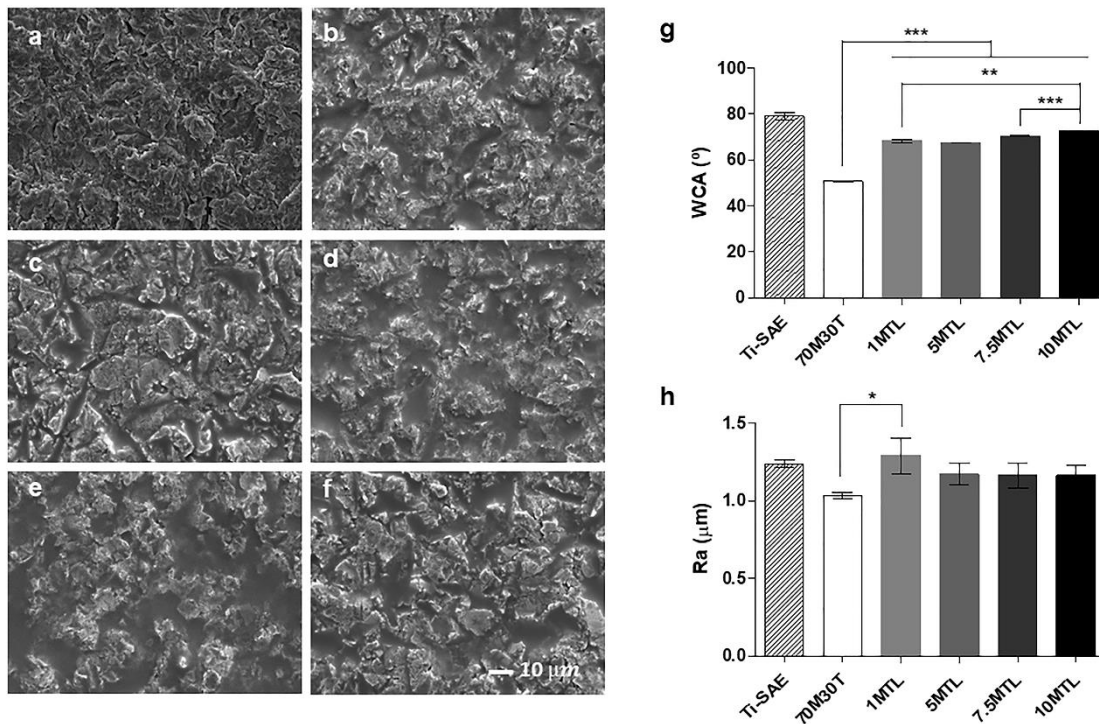
255 Based on the normal distribution and equal variance assumption test, the data were analyzed via
256 one-way analysis of variance (ANOVA) with Newman-Keuls post hoc test and expressed as mean

257 \pm standard deviation (SD). Statistical analysis was performed using GraphPad Prism 5.04
258 software (GraphPad Software Inc., La Jolla, CA, USA). The differences between 70M30T and
259 70M30T with different concentrations of MLT were considered statistically significant at $p \leq 0.05$
260 (*), $p \leq 0.01$ (**) and $p \leq 0.001$ (***).

261 3. Results

262 3.1. Physicochemical characterization

263 The sol-gel materials with MLT were successfully synthesized and well-adhering coatings were
264 obtained as it can be observed in SEM micrographs (**Figure 1**). **Figure 1g** displays the contact
265 angle measurements. With the addition of MLT to 70M30T, there was a significant increase of
266 the contact angle in a dose-response manner. Regarding the roughness, with the incorporation of
267 MLT, there was an increase of Ra when compared to 70M30T; however, there were no statistical
268 differences between the coatings with distinct amount of MLT (**Figure 1h**).



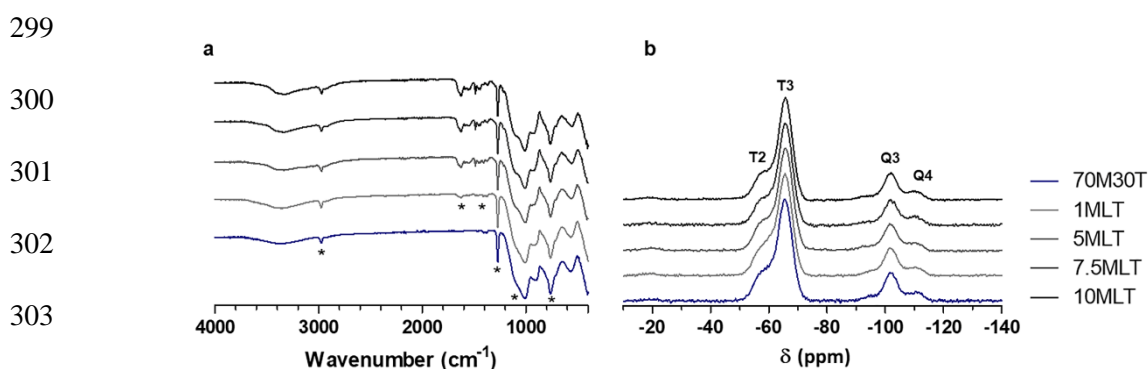
269
270 **Figure 1:** SEM microphotograph of SAE-Ti (a), 70M30T (b), 1MLT (c), 5MLT (d), 7.5MLT (e) and
271 10MLT (f) and contact angle (WCA; g) and average roughness (Ra; h). Results are show as mean \pm SD.
272 The asterisks ($p \leq 0.05$ (*), $p \leq 0.01$ (**), and $p \leq 0.001$ (***)) indicate statistical differences in relation to
273 70M30T without melatonin (MLT).

274 3.1.1. FT-IR analysis

275 Sol-gel materials with different percentages of MLT were chemically characterized using FT-IR.
276 The obtained spectra are shown in **Figure 2a**. All samples presented bands between 400 and 1200
277 cm^{-1} . The hydrolysis-condensation reaction were correctly carried out, as it was detected the

278 presence of siloxane chain characteristic signals. The bands with the Si-O-Si appear proximally
 279 at 1090 cm^{-1} (asymmetric tension [19]), 770 cm^{-1} and 440 cm^{-1} (symmetrical tension and vibration
 280 of deformation [20]). However, the condensation was not complete as bands at 970 cm^{-1} and 540
 281 cm^{-1} related to the Si-OH bond of silanol groups were detected. The band related with the OH
 282 groups were observed around 3400 cm^{-1} and can be associated with the presence of water in the
 283 sol-gel structure [21]. The bands around 3000 cm^{-1} indicate the presence of C-H bonds [21],
 284 corresponding to the organic part of the MTMOS that has a methyl group (non-hydrolysable).
 285 The band is composed by two peaks corresponding to vibrations of asymmetrical and symmetrical
 286 tension of the bond C-H. The bond associated to the Si-CH₃ group appears around 1275 cm^{-1} [22].
 287 These methyl-associated signals show that the integrity of organic species has been maintained
 288 after processing. All identified signals are maintained and display similar intensity when the MLT
 289 is incorporated into the sol-gel. However, the materials with MLT show bands between 1500-
 290 1600 cm^{-1} , which corresponds to the CO group present in this molecule[23]. In addition, the
 291 spectra of these materials show bands at 1610 cm^{-1} and 1555 cm^{-1} , which correspond to N-H and
 292 C-N bounds present in MLT, correspondingly [20]. The intensity of these bands is slightly more
 293 intense as the amount of melatonin increases.

294 **Figure 2b** represents ²⁹Si solid NMR spectra of 70M30T and 70M30T supplemented with MLT.
 295 These spectra show Tⁿ signals from MTMOS and Qⁿ signals from TEOS. The MTMOS spectra
 296 show T² and T³ signals with higher intensity of T³. Additionally, the spectra show Q³ and Q⁴ from
 297 TEOS, with a signal more intense in Q³. It seems that the addition of MLT to the sol-gel network
 298 did not affect the final crosslinking degree of structure.



304 **Figure 2:** FT-IR spectra (a) and Si-NMR (b) of 70M30T with different concentrations of melatonin (MLT).

305

306

307 3.1.2. Hydrolytic degradation

308 **Figure 3a** shows the hydrolytic degradation (mass loss) of all materials during 56 days. All
 309 materials degraded and showed a significant mass loss during the first seven days. During the
 310 following days and until the end of experiment, all materials lost weight in a more gradual way.

311 In the case of 70M30T, the mass loss was small (up to 16%), while the materials with MLT
312 showed a higher weight loss. In these coatings, the degradation increased as the percentage of
313 MLT in the network increased. Thus, the 10MLT showed the highest degradation in all materials
314 studied.

315 **3.1.3. Silicon and melatonin liberation**

316 **Figure 3b** shows the liberation of silicon (Si released in mg L^{-1}) of all materials in study. All
317 materials showed a significant Si liberation during the first week. The base material 70M30T and
318 1MLT presented a similar liberation rate, reaching its maximum at 3 weeks. For the rest of the
319 materials, the liberation was more gradual over the two months of the assay. Similarly, to the
320 hydrolytic degradation, the material with higher concentration of MLT released more Si (12.5 mg
321 Si L^{-1} in 10MLT in two months of assay). **Figure 3c** shows MLT liberation for all materials. In
322 similarity to the previously described parameters, MLT release showed a dose-response rate *i.e.*
323 the material with the highest percentage (10MLT) presented the highest liberation of MLT.
324 Considering the liberation kinetics, MLT was released faster in the first 72 h and, for this time
325 point onward, it had a liberation rate almost constant until the end of the assay (336 h) in all
326 materials.

327

328

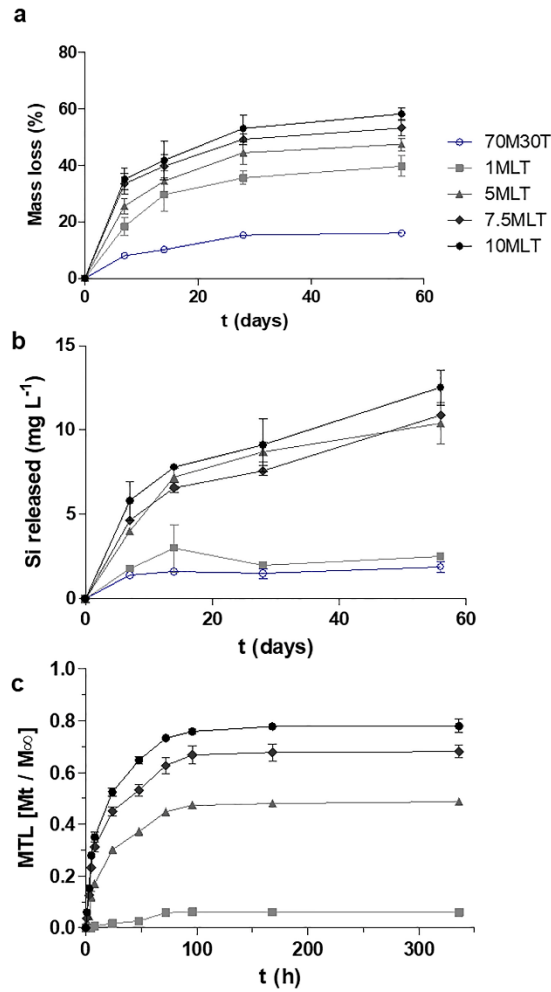
329

330

331

332

333



344

345

Figure 3: Hydrolytic degradation (a) of the sol-gel coating and kinetic liberation of silicon (b) and MTL (c) from the sol-gel coating through time.

346

3.2. *In vitro* assays

347

3.2.1. Cytotoxicity, cell proliferation and ALP activity

348

349

350

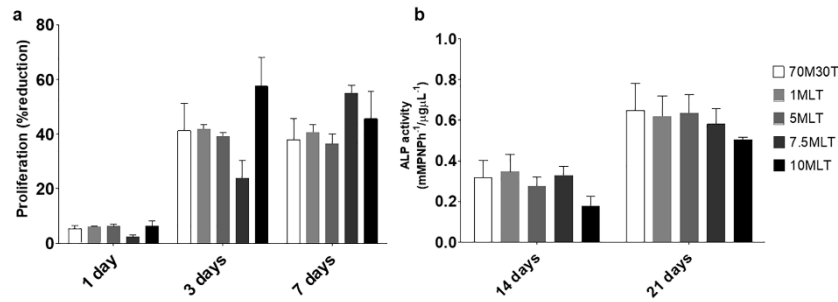
Neither of the materials in study was cytotoxic (data not shown). Cell proliferation and ALP activity assays did not show significant differences between the 70M30T with or without melatonin (**Figure 4**) in any measuring points.

351

352

353

354
355
356
357
358

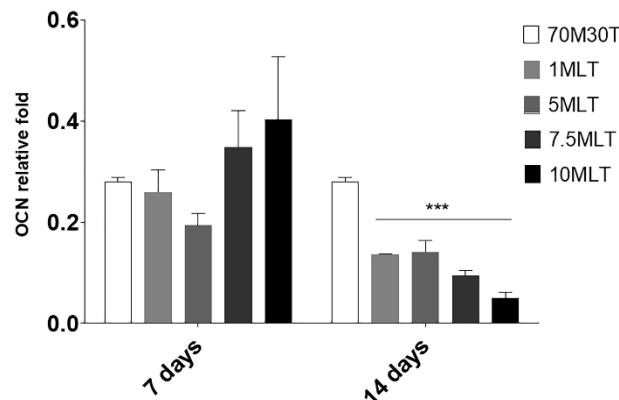


359 **Figure 4:** MC3T3-E1 *in vitro* assays: a) cell proliferation at 1, 3 and 7 days and b) ALP activity at 14 and
360 21 days. Results are show as mean ± SD.

361 3.2.2. Relative gene expression

362 The expression of osteogenic markers of the MC3T3-E1 cells cultured onto the distinct
363 formulations is shown in **Figure 5**. At 7 days, OCN expression levels showed a tendency to
364 increase in all materials with MLT, except 5MLT. After 14 days, all materials with MLT show a
365 significant decrease of this marker expression.

366
367
368
369
370
371
372

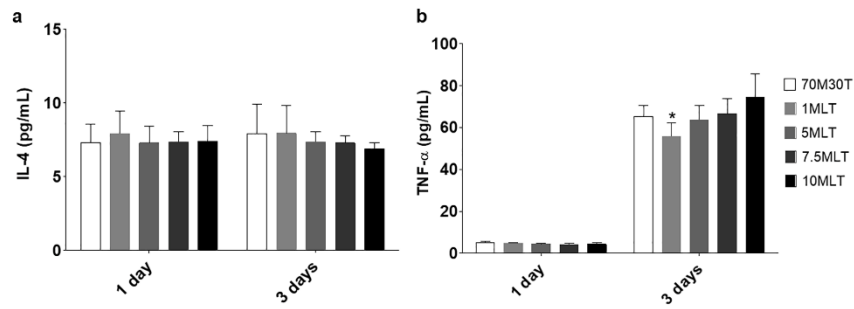


373 **Figure 5:** Relative gene expression of osteocalcin (OCN) in MC3T3 at 7 and 14 days. Results are show as
374 mean ± SD. The asterisks ($p \leq 0.001$ (***)) indicate statistical differences in relation to 70M30T without
375 melatonin (MLT).

376 3.2.3. Cytokine quantification by ELISA

377 To evaluate the effect of the materials with MLT on the inflammatory response, the secretion of
378 anti (IL-4) and pro-inflammatory (TNF- α) cytokines by RAW264.7 macrophage was quantified
379 at 1 day and 3 days. The secretion of IL-4 did not show differences at any of the times measured
380 in any of the materials tested (**Figure 6a**). In the case of TNF- α , the profile was similar at 1 day
381 for all materials (**Figure 6b**). After 3 days of culture, there is a general increase of the production
382 of this cytokine; however is significantly lower in 1%MLT when compared to the 70M30T
383 coating.

384
385
386
387
388

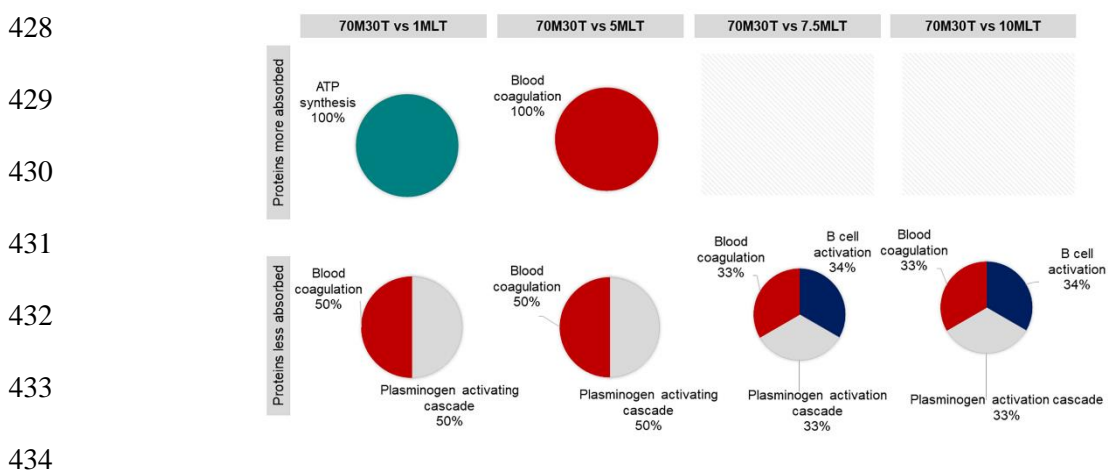


389 **Figure 6:** Cytokine quantification by ELISA in RAW264.7 at 1 and 3 days: (a) IL-4 and (b) TNF- α . Results
390 are show as mean \pm SD. The asterisk ($p \leq 0.05$ (*)) indicates statistical differences in relation to 70M30T
391 without melatonin (MLT).

392 3.2.4. Proteomic analysis

393 The eluted proteins were analyzed by LC-MS/MS, followed by identification with Progenesis QI
394 software and DAVID system. Comparing between MLT-enriched and the base sol-gel material,
395 26 proteins were differentially adsorbed in the materials with MLT (**Supplementary Table 1**).
396 The formulation with 10MLT shows the higher amount of differently adsorbed proteins, with 16
397 proteins being less adsorbed onto its surface and five showing more affinity. Among the proteins
398 with decreased adsorption, five are related with the complement system (CO7, IC1, CO5, CO8A,
399 and CO9). On the other hand, these surfaces lead to a higher adsorption with CXCL7, which plays
400 a crucial role in neutrophil recruitment. Also related with immunological responses, the surface
401 1MLT and 5MLT showed a higher affinity with IGHA2, while 7.5MLT differentially adsorbed
402 CO5, IC1, CO8A and CXCL7. The glycoproteins VTCN and SEPP1 were significantly less
403 adsorbed in the material with 10MLT, while HEMO show higher affinity with the materials with
404 1MLT, 5MLT and 10MLT. VTNC is known to inhibit/regulate the complement system
405 activation. Depending on the concentration of MLT, the materials adsorbed less apolipoproteins
406 (APOA-I, APOF, APOL1 and APOC4) and PON1. These proteins are related to the metabolism
407 of high-density lipids. Regarding the coagulation process, HRG, HBB, PLMN and KLKB1 were
408 differentially adsorbed: HRG was more adsorbed in 1MLT, while KLKB1 was more adsorbed in
409 5MLT. In 7.5MLT and 10MLT proteins related with this process presented less affinity with these
410 materials. Additionally, all materials except 7.5MLT showed differential affinity with A2GL, a
411 protein related with the angiogenesis processes. The materials 1MLT and 5MLT adsorbed more
412 of this protein, while 10MLT adsorbed less. ITIH2, ITIH4 and ITIH1, proteins from the inter- α -
413 trypsin inhibitor family related with hyaluronan metabolic process, were less adsorbed in the
414 materials with 10MLT. ATPA, a mitochondrial membrane complex that produces ATP from
415 ADP, was significantly more adsorbed in 1MLT. **Table 1** summarizes the most relevant proteins
416 related with immune responses, coagulation and angiogenesis processes found differentially
417 adsorbed onto each material surface.

418 PANTHER analysis was used to associate the differentially adsorbed proteins with their functions
 419 in distinct biological pathways. **Figure 7** shows pie-chart diagrams of the biological processes
 420 related with the proteins differentially adsorbed onto each surface when compared with 70M30T
 421 without MLT. ATP synthesis, blood coagulation, plasminogen activation, and B cell activation
 422 where the cascades identified and varied according to the concentration of MLT employed. In
 423 general, all materials showed less adsorbed proteins associated with blood coagulation,
 424 plasminogen activation; also, at higher concentrations of MLT (7.5 and 10), there was a general
 425 decrease of proteins associated with B cell activation pathways. Only the materials 1MLT and
 426 5MLT showed a significantly higher adsorption of proteins associated with biological process:
 427 ATP synthesis (1MLT) and blood coagulation (5MLT).



435 **Figure 7:** PANTHER diagram of the pathways associated with the proteins differentially adherent to MLT
 436 enriched coatings in comparison with 70M30T without MLT.

437 **Table 1.** Summary of the proteins of interest differentially adsorbed related with immune, coagulation and
 438 angiogenesis process differentially adsorbed onto each material surface when compared with 70M30T
 439 without MLT. MLT/70M30T ratios are shown between parentheses; red indicates more adsorbed and green
 440 indicates less adsorbed.

	70M30T vs 1MLT	70M30T vs 5 MLT	70M30T vs 7.5 MLT	70M30T vs 10 MLT
Immune				
				CO7 (0.46) IC1 (0.49) CO5 (0.57) VTNC (0.64) CO9 (0.66) CXCL7 (2.45)
	IGHA2 (2.56)	IGHA2 (2.83) CXCL7 (1.65)	CO5 (0.66) CO8A (0.66) CXCL7 (2.67)	
Angiogenesis and coagulation				
	HRG (1.60) A2GL (3.48)	A2GL (4.46) KLKB1 (2.91)	HBB (0.63)	HRG (0.36) A2GL (0.43) HBB (0.46) PLMN (0.51)

441 **4. Discussion**

442 The aim of study was to develop and characterize a sol-gel coating (70M30T) supplemented with
443 different percentages of MLT. Melatonin has a wide variety of biological actions and its well-
444 described properties have made it an attractive molecule for application in delivery systems in
445 dentistry and regenerative medicine[24].

446 The incorporation of MLT onto the 70M30T base introduced physicochemical changes in the
447 surface properties, such as wettability. The contact angle significantly increased in relation the
448 base regardless the concentration of MLT, surely by the organic character of this molecule.
449 Regarding the material roughness, there is only a significant increase when comparing 70M30T
450 with 1MLT. The ²⁹Si solid NMR shows that the incorporation of MLT did not affected the
451 formation of the sol-gel network and FTIR analysis show that it is present in the material. The
452 hydrolytic degradation and the Si release increased in a dose-response manner with the amount
453 of MLT incorporated in the network. This can be related with liberation of MLT that also
454 presented an increasing dose-response pattern depending on the amount of MLT initially added
455 into the coating.

456 In cancer cells, the inhibitory effect of this MLT on cell proliferation is well documented [25]. In
457 osteoblasts (hFOB 1.19), MLT showed an inhibitory effect on proliferation in a time dependent
458 manner, acting in genes related with cell division cycle[26]. Zhang et al.[17] showed that MLT
459 encapsulated in PLGA microspheres does not affect proliferation of hMSCs at 1, 3 and 6 days,
460 which is in accordance with our results. To understand how MLT affects the mineralization of
461 osteoblasts, ALP activity assay was performed. Our results show that MLT did not significantly
462 affect ALP activity at 14 and 21 days. Previous studies have showed MLT can increase ALP
463 activity in MC3T3-E1 at 14 days [27] or with 50 nM of MLT for 3 days [8]; however, these
464 findings are for when cultures are directly treated with the compound and at short times of
465 incubation (<14 days) with MLT. On the other hand, Zhang et al. [17] presented a significantly
466 higher ALP activity in MLT encapsulated microspheres at 12 days. With this, further studies are
467 needed to understand how MLT affects cells in long-term exposition (>14 days).

468 The LC-MS/MS characterization of the proteins layers identified 26 proteins that were
469 differentially absorbed in the materials with MLT. How and which proteins were adsorbed onto
470 each surfaces depended on the amount of MLT incorporated on the sol-gel network. These
471 proteins have functions associated with distinct biological pathways as shown in the PANTHER
472 analysis. Apolipoproteins APOA-I, APOF, APOL1 and APOC4 were generally less adsorbed
473 onto the surfaces with MLT. These proteins are known for their role in the metabolism of lipids,
474 this protein family might also play a role in inhibiting complement system activation [28]. APOA-

475 I is a major component of HDL that has been shown to inhibit LPS induced release of cytokines
476 in monocytes [29], revealing an anti-inflammatory potential.

477 In addition, it was found a differential adsorption of complement system proteins. In the materials
478 with 7.5MLT and 10MLT, we could observed a decrease on the adsorption of complement C5
479 (CO5), complement component C8 alpha chain (CO8A), complement component (CO7) and
480 component complement (CO9). The activation of C5 initiates an assembly with late-phase
481 complement components, such as C6, C7, C8 and C9, leading to the formation of C5-C9 complex,
482 a multimolecular structure that leads to the formation of the lytic complex that will be responsible
483 for the target cell lysis [30]. This is in agreement with the analysis PANTHER, which shows that
484 the proteins less adsorbed by these materials have functions associated with B cell activation. The
485 distinct complement pathways originate C3 and C4 fragments, which bind to complement
486 receptors CD21 and CD35, whose co-expression is limited to B cells and lead to the enhancement
487 of the activity of these cells [31,32]. On the other hand, vitronectin (VTNC) was less adsorbed in
488 the materials with 10MLT. This protein has been described as an inhibitor of complement system
489 action in bodily fluids [33]. Thus, the lower adsorption of complement proteins associated with
490 the lower adsorption of VTNC can explain how the release of TNF- α and IL-4 cytokines by
491 macrophage in contact with the 10MLT showed no statistical differences with respect to the base
492 coating. Although, the anti-inflammatory potential of MLT is well described [11,34,35], its
493 application in biomaterials can be dependent in the amount of hormone released by the material
494 over time and further studies are needed.

495 Coagulation and angiogenesis are key processes in bone regeneration. Proteomic analysis showed
496 that MLT enriched materials differently adsorbed proteins related with both of these processes.
497 In this sense, A2GL, protein implicated in angiogenesis [36], was found to be more adsorbed onto
498 the coatings 1MLT and 5MLT, but then, reduced its affinity with respect to the base material
499 when 10% of MLT was incorporate. *In vitro*, MLT was reported to inhibit angiogenesis in cancer
500 cells [37,38]. On the other hand, Ramírez-Fernandez et al. [39] reported that MLT promoted this
501 process in rabbit tibiae following implantation of melatonin implants.

502 Regarding the coagulation process, HRG, which modulates various components in the
503 coagulation cascade, such as heparin, increased its affinity for 1MLT. Similarly, KLKB1 was
504 significantly more adsorbed onto the material 5MLT. This protein activates the coagulation
505 cascade through the intrinsic pathway [40]. However, both KLKB1 and HRG reduced the affinity
506 by the material when a 10% of MLT was added.

507 Fibrinolysis is a highly regulated enzymatic process of clot removal tightly related with blood
508 coagulation [41]. PLMN, protein found less adsorbed onto 10MLT, has a role in tissue
509 regeneration by dissolving preformed fibrin clots and extracellular matrix components allowing

510 tissue remodeling [42]. These adsorption patterns are corroborated with PANTHER analysis,
511 which showed a general decrease in proteins with functions related with blood coagulation and
512 plasminogen activation.

513 MLT has a complex biological role and its potential effect on important pathways, such as
514 inflammation, coagulation and angiogenesis, in the early stages of tissue regeneration, can
515 determine how these processes will be carried out around an implant. However, its specific
516 mechanism of action, timings and doses needed to produce significant cellular effects still need
517 further studies.

518 **5. Conclusions**

519 In this article, we developed new coatings with MLT to be applied in titanium dental implants
520 using hybrid sol-gel network as a release vehicle. The addition of MLT changed the superficial
521 parameters of the coatings, with the coatings supplemented with the hormone showing a lower
522 hydrophilia when compared to the base material. These materials revealed to be not cytotoxic.
523 However, osteoblastic cells did not show an improvement in the capacity of proliferation and
524 mineralization *in vitro* when exposed to the coatings. The proteomic analysis of protein adsorption
525 onto the materials showed differences in the adsorption patterns in proteins associated with the
526 complement pathway when MLT added and in a dose-response manner. This behavior can explain
527 the liberation of TNF- α , which was significantly lower in the 1MLT composition. In addition, it
528 was found differences in adsorption of proteins related with coagulation and angiogenesis, which
529 points out a possible effect of MLT in the activation and development of these pathways.

530 **6. Acknowledgments**

531 This work was supported by MINECO [MAT MAT2017-86043-R; RTC-2017-6147-1],
532 Universitat Jaume I under [UJI-B2017-37; POSDOC/2019/28], Generalitat Valenciana
533 [GRISOLIAP/2018/091], University of the Basque Country under [UFI11/56] and Basque
534 Government under [PRE_2017_2_0044]. CIC bioGUNE is supported by Basque Department of
535 Industry, Tourism and Trade (Eortek and Elkartek programs), the Innovation Technology
536 Department of the Bizkaia County; The ProteoRed-ISCI (Grant PRB3 IPT17/0019); CIBERehd
537 Network and Severo Ochoa Grant (SEV-2016-0644). Authors would like to thank Antonio Coso
538 (GMI-Ilerimplant) for their inestimable contribution to this study, and Raquel Oliver, Jose Ortega
539 (UJI) and Iraide Escobes (CIC bioGUNE) for their valuable technical assistance.

540 **7. References**

541 [1] R. Smeets, B. Stadlinger, F. Schwarz, B. Beck-Broichsitter, O. Jung, C. Precht, F. Kloss,
542 A. Gröbe, M. Heiland, T. Ebker, Impact of Dental Implant Surface Modifications on
543 Osseointegration, *Biomed Res. Int.* 2016 (2016) 1–16. doi:10.1155/2016/6285620.

- 544 [2] J.A. Oshiro Junior, M. Abuçafy, E. Manaia, B. Da Silva, B.G. Chiari-Andréo, L.A.
545 Chiavacci, Drug delivery systems obtained from silica based organic-inorganic hybrids,
546 *Polymers (Basel)*. 8 (2016) 91. doi:10.3390/polym8040091.
- 547 [3] M. Martínez-Ibáñez, M.J. Juan-Díaz, I. Lara-Saez, A. Coso, J. Franco, M. Gurruchaga, J.
548 Suay Antón, I. Goñi, Biological characterization of a new silicon based coating developed
549 for dental implants, *J. Mater. Sci. Mater. Med.* 27 (2016). doi:10.1007/s10856-016-5690-
550 9.
- 551 [4] S. Maria, A. Witt-Enderby, P, Melatonin effects on bone: Potential use for the prevention
552 and treatment for osteopenia, osteoporosis, and periodontal disease and for use in bone-
553 grafting procedures, *J. Pineal Res.* 56 (2014) 115–125. doi:10.1111/jpi.12116.
- 554 [5] J.A. Roth, B.G. Kim, W.L. Lin, M.I. Cho, Melatonin promotes osteoblast differentiation
555 and bone formation, *J. Biol. Chem.* 274 (1999) 22041–22047.
556 doi:10.1074/jbc.274.31.22041.
- 557 [6] S. Sethi, N.M. Radio, M.P. Kotlarczyk, C.-T. Chen, Y.-H. Wei, R. Jockers, P.A. Witt-
558 Enderby, Determination of the minimal melatonin exposure required to induce osteoblast
559 differentiation from human mesenchymal stem cells and these effects on downstream
560 signaling pathways, *J. Pineal Res.* 49 (2010) 222–238. doi:10.1111/j.1600-
561 079X.2010.00784.x.
- 562 [7] L. Zhang, P. Su, C. Xu, C. Chen, A. Liang, K. Du, Y. Peng, D. Huang, Melatonin inhibits
563 adipogenesis and enhances osteogenesis of human mesenchymal stem cells by suppressing
564 PPAR γ expression and enhancing Runx2 expression, *J. Pineal Res.* 49 (2010) 364–372.
565 doi:10.1111/j.1600-079X.2010.00803.x.
- 566 [8] K.H. Park, J.W. Kang, E.M. Lee, J.S. Kim, Y.H. Rhee, M. Kim, S.J. Jeong, Y.G. Park, S.
567 Hoon Kim, Melatonin promotes osteoblastic differentiation through the BMP/ERK/Wnt
568 signaling pathways, *J. Pineal Res.* 51 (2011) 187–194. doi:10.1111/j.1600-
569 079X.2011.00875.x.
- 570 [9] Z. Ping, Z. Wang, J. Shi, L. Wang, X. Guo, W. Zhou, X. Hu, X. Wu, Y. Liu, W. Zhang,
571 H. Yang, Y. Xu, Y. Gu, D. Geng, Inhibitory effects of melatonin on titanium particle-
572 induced inflammatory bone resorption and osteoclastogenesis via suppression of NF- κ B
573 signaling, *Acta Biomater.* 62 (2017) 362–371. doi:10.1016/j.actbio.2017.08.046.
- 574 [10] M. Kadena, Y. Kumagai, A. Vandenberg, H. Matsushima, H. Fukamachi, N. Maruta, H.
575 Kataoka, T. Arimoto, H. Morisaki, T. Funatsu, H. Kuwata, Microarray and gene co-
576 expression analysis reveals that melatonin attenuates immune responses and modulates

- 577 actin rearrangement in macrophages, *Biochem. Biophys. Res. Commun.* 485 (2017) 414–
578 420. doi:10.1016/j.bbrc.2017.02.063.
- 579 [11] Y. Xia, S. Chen, S. Zeng, Y. Zhao, C. Zhu, B. Deng, G. Zhu, Y. Yin, W. Wang, R.
580 Hardeland, W. Ren, Melatonin in macrophage biology: Current understanding and future
581 perspectives, *J. Pineal Res.* 66 (2019) 1–21. doi:10.1111/jpi.12547.
- 582 [12] R. Hardeland, Melatonin and inflammation—Story of a double-edged blade, *J. Pineal Res.*
583 65 (2018) 1–23. doi:10.1111/jpi.12525.
- 584 [13] N. Araújo-Gomes, F. Romero-Gavilán, I. García-Arnáez, C. Martínez-Ramos, A.M.
585 Sánchez-Pérez, M. Azkargorta, F. Elortza, J.J. Martín de Llano, M. Gurruchaga, I. Goñi,
586 J. Suay, Osseointegration mechanisms: a proteomic approach, *JBIC J. Biol. Inorg. Chem.*
587 23 (2018) 459–470. doi:10.1007/s00775-018-1553-9.
- 588 [14] Z. Sheikh, P.J. Brooks, O. Barzilay, N. Fine, M. Glogauer, Macrophages, foreign body
589 giant cells and their response to implantable biomaterials, *Materials (Basel)*. 8 (2015)
590 5671–5701. doi:10.3390/ma8095269.
- 591 [15] F. Romero-Gavilán, N. Araújo-Gomes, A. Cerqueira, I. García-Arnáez, C. Martínez-
592 Ramos, M. Azkargorta, I. Iloro, M. Gurruchaga, J. Suay, I. Goñi, Proteomic analysis of
593 calcium - enriched sol – gel biomaterials, *JBIC J. Biol. Inorg. Chem.* 24 (2019) 563–574.
594 doi:10.1007/s00775-019-01662-5.
- 595 [16] F. Romero-Gavilan, A.M. Sánchez-Pérez, N. Araújo-Gomes, M. Azkargorta, I. Iloro, F.
596 Elortza, M. Gurruchaga, I. Goñi, J. Suay, Proteomic analysis of silica hybrid sol-gel
597 coatings: a potential tool for predicting the biocompatibility of implants *in vivo*,
598 *Biofouling*. 33 (2017) 676–689. doi:10.1080/08927014.2017.1356289.
- 599 [17] L. Zhang, J. Zhang, Y. Ling, C. Chen, A. Liang, Y. Peng, H. Chang, P. Su, D. Huang,
600 Sustained release of melatonin from poly (lactic-co-glycolic acid) (PLGA) microspheres
601 to induce osteogenesis of human mesenchymal stem cells in vitro, *J. Pineal Res.* 54 (2013)
602 24–32. doi:10.1111/j.1600-079X.2012.01016.x.
- 603 [18] J.R. Wiśniewski, A. Zougman, N. Nagaraj, M. Mann, Universal sample preparation
604 method for proteome analysis, *Nat. Methods*. 6 (2009) 359–362. doi:10.1038/nmeth.1322.
- 605 [19] F. Romero-Gavilán, S. Barros-Silva, J. García-Cañadas, B. Palla, R. Izquierdo, M.
606 Gurruchaga, I. Goñi, J. Suay, Control of the degradation of silica sol-gel hybrid coatings
607 for metal implants prepared by the triple combination of alkoxysilanes, *J. Non. Cryst.*
608 *Solids*. 453 (2016) 66–73. doi:10.1016/j.jnoncrsol.2016.09.026.
- 609 [20] Y. Li, X. Zhao, Y. Zu, L. Wang, W. Wu, Y. Deng, C. Zu, Y. Liu, Melatonin-loaded silica

- 610 coated with hydroxypropyl methylcellulose phthalate for enhanced oral bioavailability:
611 Preparation, and in vitro-in vivo evaluation, *Eur. J. Pharm. Biopharm.* 112 (2017) 58–66.
612 doi:10.1016/j.ejpb.2016.11.003.
- 613 [21] M.J. Juan-Díaz, M. Martínez-Ibáñez, M. Hernández-Escolano, L. Cabedo, R. Izquierdo,
614 J. Suay, M. Gurruchaga, I. Goñi, Study of the degradation of hybrid sol-gel coatings in
615 aqueous medium, *Prog. Org. Coatings.* 77 (2014) 1799–1806.
616 doi:10.1016/j.porgcoat.2014.06.004.
- 617 [22] A.S. Vishnevskiy, D.S. Seregin, K.A. Vorotilov, A.S. Sigov, K.P. Mogilnikov, M.R.
618 Baklanov, Effect of water content on the structural properties of porous methyl-modified
619 silicate films, *J. Sol-Gel Sci. Technol.* 92 (2019) 273–281. doi:10.1007/s10971-019-
620 05028-w.
- 621 [23] M. Sabzichi, N. Samadi, J. Mohammadian, H. Hamishehkar, M. Akbarzadeh, O. Molavi,
622 Sustained release of melatonin: A novel approach in elevating efficacy of tamoxifen in
623 breast cancer treatment, *Colloids Surfaces B Biointerfaces.* 145 (2016) 64–71.
624 doi:10.1016/j.colsurfb.2016.04.042.
- 625 [24] S. Maria, P.A. Witt-Enderby, Melatonin effects on bone: Potential use for the prevention
626 and treatment for osteopenia, osteoporosis, and periodontal disease and for use in bone-
627 grafting procedures, *J. Pineal Res.* 56 (2014) 115–125. doi:10.1111/jpi.12116.
- 628 [25] A. Cutando, A. López-Valverde, S. Arias-Santiago, J. De Vicente, R.G. De Diego, Role
629 of melatonin in cancer treatment, *Anticancer Res.* 32 (2012) 2747–2754.
- 630 [26] L. Liu, Y. Zhu, Y. Xu, R.J. Reiter, Melatonin delays cell proliferation by inducing G 1 and
631 G 2 / M phase arrest in a human osteoblastic cell line hFOB 1 . 19, *J. Pineal Res.* (2011)
632 222–231. doi:10.1111/j.1600-079X.2010.00832.x.
- 633 [27] J.H. Son, Y.C. Cho, I.Y. Sung, I.R. Kim, B.S. Park, Y.D. Kim, Melatonin promotes
634 osteoblast differentiation and mineralization of MC3T3-E1 cells under hypoxic conditions
635 through activation of PKD/p38 pathways, *J. Pineal Res.* 57 (2014) 385–392.
636 doi:10.1111/jpi.12177.
- 637 [28] N.H. Cho, S.Y. Seong, Apolipoproteins inhibit the innate immunity activated by necrotic
638 cells or bacterial endotoxin, *Immunology.* 128 (2009) 479–486. doi:10.1111/j.1365-
639 2567.2008.03002.x.
- 640 [29] J.F.P. Berbée, L.M. Havekes, P.C.N. Rensen, Apolipoproteins modulate the inflammatory
641 response to lipopolysaccharide, *J. Endotoxin Res.* 11 (2005) 97–103.
642 doi:10.1179/096805105X35215.

- 643 [30] P. Nesargikar, B. Spiller, R. Chavez, The complement system: History, pathways, cascade
644 and inhibitors, *Eur. J. Microbiol. Immunol.* 2 (2012) 103–111.
645 doi:10.1556/eujmi.2.2012.2.2.
- 646 [31] M.C. Carroll, The complement system in regulation of adaptive immunity, *Nat. Immunol.*
647 5 (2004) 981–986. doi:10.1038/ni1113.
- 648 [32] M.C. Carroll, The complement system in B cell regulation, in: *Mol. Immunol.*, 2004: pp.
649 141–146. doi:10.1016/j.molimm.2004.03.017.
- 650 [33] T.E. Mollnes, M. Kirschfink, Strategies of therapeutic complement inhibition, *Mol.*
651 *Immunol.* 43 (2006) 107–121. doi:10.1016/j.molimm.2005.06.014.
- 652 [34] J.L. Mauriz, P.S. Collado, C. Veneroso, R.J. Reiter, J. González-Gallego, A review of the
653 molecular aspects of melatonin's anti-inflammatory actions: Recent insights and new
654 perspectives, *J. Pineal Res.* 54 (2013) 1–14. doi:10.1111/j.1600-079X.2012.01014.x.
- 655 [35] J.R. Calvo, C. Gonzalez-Yanes, M.D. Maldonado, The role of melatonin in the cells of the
656 innate immunity: A review, *J. Pineal Res.* 55 (2013) 103–120. doi:10.1111/jpi.12075.
- 657 [36] L.J. Druhan, A. Lance, S. Li, A.E. Price, J.T. Emerson, S.A. Baxter, J.M. Gerber, B.R.
658 Avalos, Leucine rich α -2 glycoprotein: A novel neutrophil granule protein and modulator
659 of myelopoiesis, *PLoS One.* 12 (2017) 1–13. doi:10.1371/journal.pone.0170261.
- 660 [37] S. Park, W. Jang, E. Yi, J. Jang, Y. Jung, J. Jeong, Y. Kim, Melatonin suppresses tumor
661 angiogenesis by inhibiting HIF-1 α stabilization under hypoxia, *J. Pineal Res.* 48 (2010)
662 178–184. doi:10.1111/j.1600-079X.2009.00742.x.
- 663 [38] K. Kim, J. Choi, I. Kang, K. Kim, C. Jeong, J. Jeong, Melatonin suppresses tumor
664 progression by reducing angiogenesis stimulated by HIF-1 in a mouse tumor model, *J.*
665 *Pineal Res.* 54 (2013) 264–270. doi:10.1111/j.1600-079X.2012.01030.x.
- 666 [39] M.P. Ramírez-Fernández, J.L. Calvo-Guirado, J. Eduardo-Maté Sánchez de-Val, R.A.
667 Delgado-Ruiz, B. Negri, G. Pardo-Zamora, D. Peñarrocha, C. Barona, J. Manuel Granero,
668 M. Alcaraz-Baños, M.P. Ramírez-Fernández, J.L. Calvo-Guirado, B. Negri, G. Pardo-
669 Zamora, J.M. Granero, J.S. E-M de-Val, R.A. Delgado-Ruiz, D. Peñarrocha, C. Barona,
670 M. Alcaraz-Baños, H. Morales Meseguer, Melatonin promotes angiogenesis during repair
671 of bone defects: a radiological and histomorphometric study in rabbit tibiae, *Clin. Oral*
672 *Investig.* 17 (2013) 147–158. doi:10.1007/s00784-012-0684-6.
- 673 [40] Y. Wu, Contact pathway of coagulation and inflammation, *Thromb. J.* 13 (2015) 17.
674 doi:10.1186/s12959-015-0048-y.

- 675 [41] J.C. Chapin, K.A. Hajjar, Fibrinolysis and the control of blood coagulation, (2014).
676 doi:10.1016/j.blre.2014.09.003.
- 677 [42] D. V. Sakharov, J.F. Nagelkerkel, D.C. Rijken, Rearrangements of the fibrin network and
678 spatial distribution of fibrinolytic components during plasma clot lysis: Study with
679 confocal microscopy, J. Biol. Chem. 271 (1996) 2133–2138. doi:10.1074/jbc.271.4.2133.
- 680